Metallography, Microstructure, and Analysis (2023) 12:246–261
https://doi.org/10.1007/s13632-023-00944-4

PEER-REVIEWED PAPER

Lead-Glazed Ceramic Fragments: Intentional Glazing or Metallurgical Accident?

S. Klein[1,2] · S. Fischer-Lechner[1,2] · C. Berthold[3] · J. Sessing[4] · T. Kirnbauer[5] · M. Zeiler[6] · W. Essling-Wintzer[7]

Received: 18 September 2022 / Revised: 13 February 2023 / Accepted: 3 March 2023 / Published online: 20 April 2023

Abstract

Ceramic fragments from an excavation by Landschaftsverband Westfalen-Lippe in 2014 around the deserted early medieval site of Brilon-Alme were subjected to archaeometric analysis. Except for one miniature object, they are coarse-grained tempered, and many of them are coated with a green-brownish glaze. The question arose whether archaeometric investigation could help identify the material, the production technique, and the nature of the glaze. Furthermore, it was of interest whether the fragments were connected to metallurgical activity in the region. Thin sections of the fragments with adhering glaze were investigated by polarized light microscopy and energy-dispersive scanning electron microscopy, both for elemental information; powder and x-ray microdiffraction for phase analysis and multi-collector inductively coupled mass spectrometry for lead isotope analysis were applied. The results from elemental, phase, and texture analysis of the glazes finally provided evidence that they are closely related to metallurgical processes of early medieval activities around Brilon.

Keywords Archaeometallurgy · Lead · Glaze · Pottery · Kiln · Brilon · Melanotekite · Hematite · Micro-XRD

Introduction

Geographical and Geological Setting

The potters kiln is situated in the Lühlingsbach valley 3 km northeast of Brilon-Alme and 3 km west of Bad Wünnenberg-Bleiwäsche (Fig. 1). Geographically, the site belongs to the eastern Sauerland region in North Rhine-Westphalia, Germany. Geologically, the region is part of the Rhenish Massif (Rheinisches Schiefergebirge), which belongs to the Rhenohercynian Zone of the Variscan belt in Central

This invited article is part of a special topical issue of the journal Metallography, Microstructure, and Analysis on Archaeometallurgy. The issue was organized by Dr. Patricia Carrizo, National Technological University—Mendoza Regional, and Dr. Omid Oudbashi, Art University of Isfahan and The Metropolitan Museum of Art, on behalf of the ASM International Archaeometallurgy Committee.

✉ S. Klein
sabine.klein@rub.de

1 Institut für Archäologische Wissenschaften, Ruhr-Universität Bochum, Am Bergbaumuseum 31, 44791 Bochum, Germany

2 Forschungsbereich Archäometallurgie, Deutsches Bergbau-Museum Bochum, Am Bergbaumuseum 31, 44791 Bochum, Germany

3 Competence Center Archaeometry – Baden-Wuerttemberg (CCA-BW), Universität Tübingen, Wilhelmstraße 56, 72074 Tübingen, Germany

4 Forschungslabor der Abt. Forschung, Deutsches Bergbau-Museum Bochum, Herner Str. 45, 44787 Bochum, Germany

5 Wissenschaftsbereich Georessourcen und Verfahrenstechnik, Technische Hochschule Georg Agricola, Herner Str. 45, 44787 Bochum, Germany

6 Außenstelle Olpe, LWL-Archäologie für Westfalen, In der Wüste 4, 57462 Olpe, Germany

7 Referat Mittelalter und Neuzeitarchäologie, LWL-Archäologie für Westfalen, An den Speichern 12, 48157 Münster, Germany

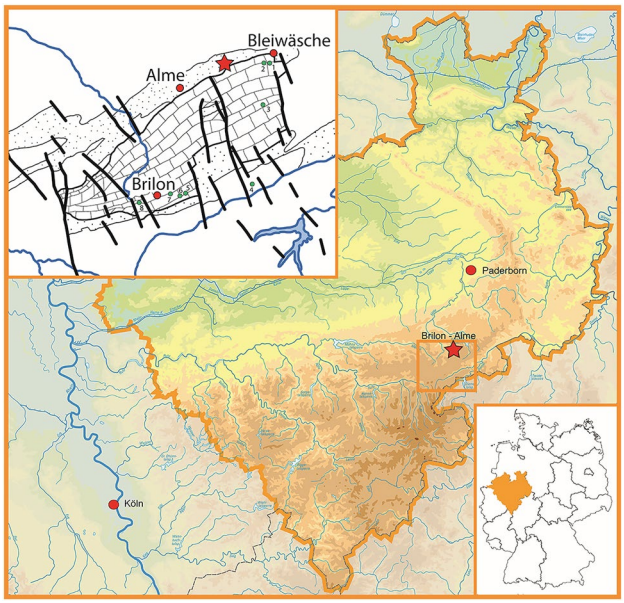

Fig. 1 Geographic location of the finding site. In close-up, the geological setting of the Brilon anticline region is sketched (modified according to [6]). Brick signature = Upper Carboniferous; Stippled signature = Lower Carboniferous. Locations 1–8: 1 = Quarry Bleiwäsche; 2 = abandoned Buchholz mine; 3 = Quarry Madfeld; 4 = Weiße Kaule; 5 = Nüllstein; 6 = Kirchloh; 7 = Kanzlei; 8 = Schlammkeule

Europe. This fold-and-thrust belt is composed of Paleozoic (Ordovician to Carboniferous) sediments and volcanic rocks which were overprinted by a very low grade metamorphism [1]. The site is situated in an approximately 17-km-long, SW–NE striking anticlinal structure, the Brilon anticline. The core of the anticline is composed of Middle to Upper Devonian biostromal and intertidal limestones with a thickness of > 1250 m [2–4].

The carbonatic rocks of the Brilon anticline host a great number of mineral veins and metasomatic deposits, predominantly bound to NNW–SSE striking normal faults [5, 6]. In addition to barren calcite, barite, and quartz veins, dozens of Pb-Zn-Fe mineralizations are known. The main ore minerals are galena, calamine, and limonite/goethite. Field observations show that the mineralizations are undeformed and therefore of post-Variscan age [6]. K-Ar dating of illites (< 2 mm) related to the calcite veins of the Eichholz mine near Thülen suggests a mineralization age of ~ 170 Ma (Middle Jurassic) [7], which is in good agreement with other post-Variscan mineralization ages in other parts of the Rhenish Massif [8]. Mining took place predominantly in the oxidation zone [5], so that parts of the primary sulfides (galena, sphalerite/schalenblende, pyrite) are present in weathered form (cerussite, calamine, limonite/goethite). Galena generally is silver-poor; Ag measurements of 27 galena samples from the Brilon mining district reveal low silver contents of 90 ppm at maximum [6, 9]. The silver-poor galena was an important raw material in the production of lead glazes for ceramic products and was therefore named "glaze ore" ("Glasurerz," "Bleiglasurerz") [10]. Coarse-grained galena occurs in calcite, barite, and quartz veins, but up to > 100 kg heavy masses also were found in clays ("Letten") accompanying the veins and in clay fillings of dolines and other karst sediments ([5], own observations). Galena and clays can therefore occur side by side in the former Brilon mining district.

Evidence for galena exploitation occurs already by Roman time (end of the first century CE) and again, in the eleventh century CE [11, 12], which was confirmed by a radiocarbon dating of one charcoal sample [13]. A large number of pinge fields, tapping and forging slags prove extensive ore processing of lead. The produced lead was used for many purposes such as lead anchors, lead pipes, weights, and other daily use. The deposits, the so-called lead glaze veins, were excellently suited for use as a glaze component for ceramic products. The lead in glazes acts as both a network former and a network converter, so lead glazes do not require a complicated recipe to work. The glazing temperatures can also be kept at a very low level.

Archaeological Setting

The fragments are from an archaeological site in the Lühlingsbachtal, which is located approximately 10 km from Brilon. Archaeological site and excavation are described in detail by Essling-Wintzer et al. 2016. The Lühlingsbachtal is surrounded by the mountain range of the Buchholz, a stream runs through the valley, and the slopes are arboreous. There is an extensive field of Pingen [14]. Local amateur historians discovered a vast number of ceramic findings, and likewise, misfires were identified. These suggested that not only ores were smelted at the site (as evidenced by the discovery of slag with adhering furnace walls), but also pottery was produced. An excavation during autumn/winter 2014 was to provide clarification about the condition of the soil monument, but also to localize potential pottery production. During this campaign, remains of a furnace were found. The kiln dome may already have been dismantled after the last fire for opening to remove the content and subsequently weathered. The furnace plate, on the other hand, was torn away by plowing. The lower parts of the furnace, the working pit and the firing chamber, were deeply carved out of the bedrock, which is why they had not been destroyed by plowing and could be excavated. The kiln was a horizontal cross-droughted two-chambered (fireplace and firing chamber) kiln, as supposed from field evidence. The combustion and firing chambers were separated from each other by a clay construction to transfer the hot air more homogeneously into the combustion chamber. The kiln was oriented in the field

so that natural wind could support the fire. An important finding in the excavation was a waste dump next to the kiln with lots of clay fragments. These included rim sherds, body sherds, bottom sherds from different kinds of ceramics, but also miniature vessels and some round-bottomed jars and bowls. The sherds are of different thickness and from oxidic firing. A large number, especially the miniature vessels and bowls, have remnants of glazes on the outer and/or the inner side, which was suspected to be lead glazing. The color of the glazes varies from light yellowish green to red–brown. Based on the thin-walled low-fired and unglazed sherds from round-bottomed jars, which remained in the furnace from the latest furnace cycle, it can be determined when the kiln was last in operation. Their typology, especially the protruding rims with grooves and the rounded rim end, indicates the late twelfth/early thirteenth century [13]. This allows the conclusion that as early as the thirteenth century lead-glazed earthenware was produced in the region around Brilon-Alme. Ore mining (lead ore, calamine) was active until the 1880s [5], and calcite deep mining lasted until the end of the twentieth century.

The Materials

The 13 fragments from the waste dump were provided by the Landschaftsverband Westfalen-Lippe (LWL). Eight of them (Figs. 2 and 3; Table 1) were subject to material investigation. Four unglazed sherds and a miniature vessel were excluded; the latter because it was a distinctly different type and pottery and appeared too precious to be subjected to destructive analysis. The examined fragments consist of coarsely fired clay and glaze attachments. Three samples (A45170048_4; _8b; _8c) were archaeologically identified as crucible rim fragments. One is described as a ceramic wall fragment (A45170048_8a) and two (A45170048_11b; _11d) as furnace wall fragments. Two samples are lumps of undefined shape (A45170048_11e; _11f), which cannot be assigned to a ceramic typology or function. It is obvious that they are all clearly different from the thin-walled, round-bottomed vessels from the kiln, and the archaeological address as crucibles or furnace walls suggests a metallurgical context. The glaze varies greatly in extent and coloration and is found on both exterior and interior surfaces. Some are smoothly coated; others adhere as silvery-gray drips.

For comparison with local ore, a sample of post-Variscan galena (AKZ 4518, 52:007) from a medieval galena mine [15] in the Buchholz Forest 1.5 km southwest of Bad Wünnenberg-Bleiwäsche (UTM 478,244/5701618), less than 2 km away from the archaeological site, was analyzed. The archaeological site was recovered by LWL Archaeology for Westphalia in 2017 from an area that was not remolded by mining operations.

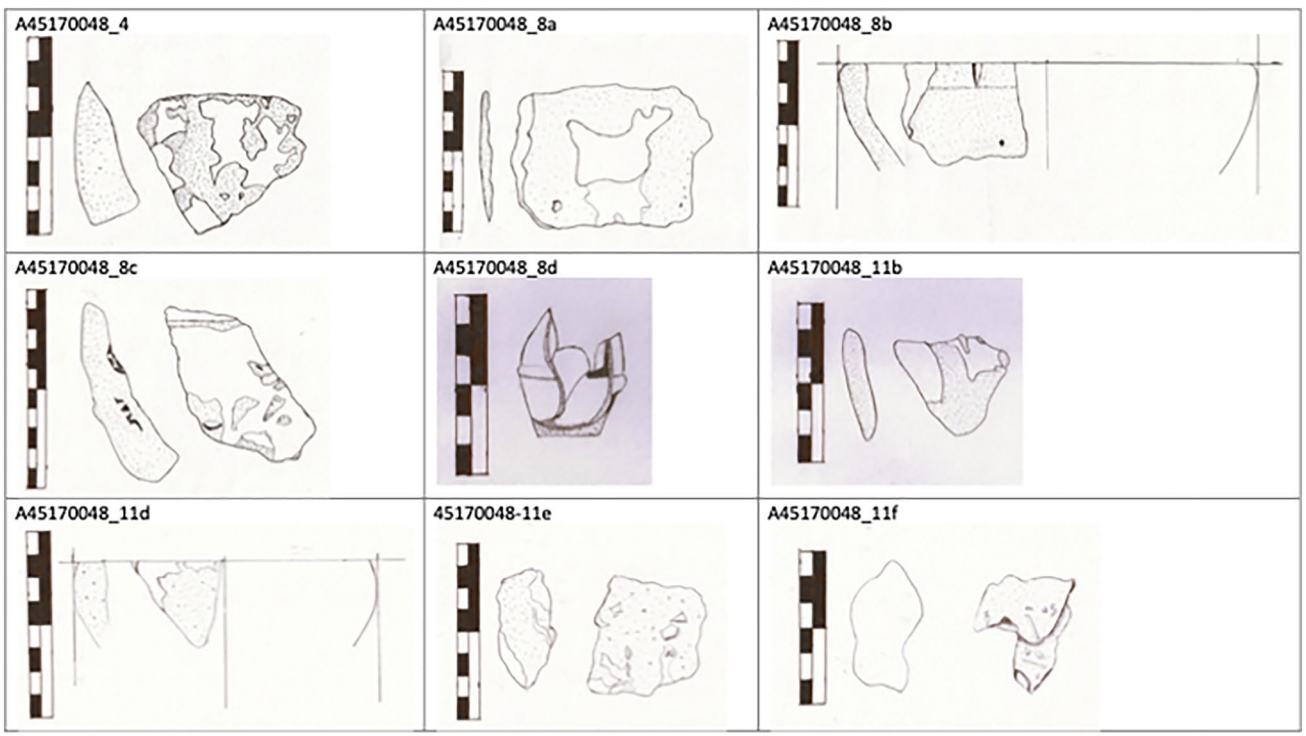

Fig. 2 Drawings of the glazed objects (by S. Fischer-Lechner)

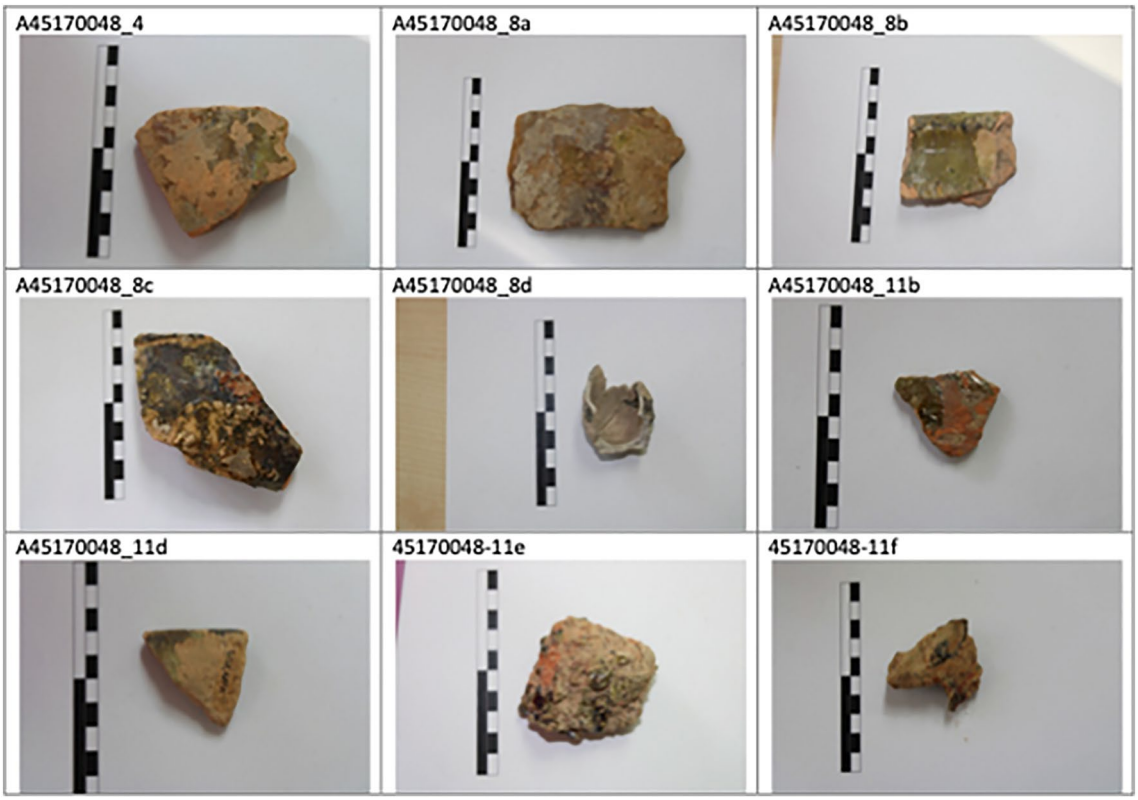

Fig. 3 Macrophotographs of the glazed objects

Table 1 Ceramic fragments from the waste dump. Inventory numbers and object details

Item number	Type	Height in mm	Width in mm	Size in mm	Weight in g	Temper	Glazing	Glazing color
A45170048_4	Rim fragment (crucible)	56	66	19.76	64	Coarse	Remains on surface	Olive green
A45170048_8a	Ceramic wall fragment	98	69	5.47	51	Coarse	Remains on surface and reverse side	Brownish
A45170048_8b	Rim fragment (crucible)	57	49	13.15	46	Coarse	Remains on surface, reverse side completely	Olive green
A45170048_8c	Rim fragment (crucible)	106	55	20.4	118	Coarse	Remains on surface	Brownish green
A45170048_8d	Miniature jar	34	43	25	10	Fine	Remains outside and inside	Dark brown
A45170048_11b	Rim fragment (furnace wall)	45	36	8.68	13	Coarse	Remains on surface, reverse side brown	Olive green
A45170048_11d	Rim fragment (furnace wall)	40	39	13.78	16	Coarse	Remains on surface, reverse side completely	Olive green
A45170048_11e	Lump	68	56	36	111	Coarse	Drips	Silvery-gray drips
A45170048_11f	Lump	40	51	26.41	34	Coarse	Drips, metallic inclosures	Silvery-gray drips

Metallurgical Background to Research

Apart from ceramic glazes in pottery production, coatings of amorphous silica-rich layers have been observed repeatedly in metallurgical contexts. An outstanding example is known from the copper metallurgy at Ras en-Naqab in Jordan. Here, white sandstone and dolomitic limestone lining were used to build up copper smelting furnaces, and the excavated lining fragments are covered with green, red, or black glazes [16]. Comparable glazes formed over sandstone blocks in smelting furnaces and as glass coatings of crucibles are reported [16–18]. A special feature, which does not require silica-rich glazing powder, is quartz ceramic over which intense blue glazes can be produced by chemical interaction between the quartz ceramic and copper pigment or copper vapors [19]. It is also described that the Romans added litharge, a metallurgical by-product of lead-silver smelting as a coloring agent for opaque yellow and green Roman glasses [20].

All these examples show that glazes occurring do not necessarily have a deliberate pottery background, but can also have a metallurgical context. It is obvious that the fragments coated with lead glazes from Brilon must have a relationship to the metallurgy of the lead-rich galena since it was exploited and smelted exactly in the neighborhood. The archaeological classification as crucibles and the thick adhesions and drips of glaze on the lumps fit well with this idea. The following investigations could shed new light on similarities between glazes from metallurgy and pottery production.

Experimental Methods and Tests

Non-destructive and Minimally Destructive Testing

EDS–SEM

Scanning electron microscopy was carried out in the laboratories of the Deutsches Bergbau Museum in Bochum. The instrument used is a Zeiss Supra 40 VP with a field emission gun. The analyses were performed in situ on the surfaces of the ceramic fragments. Variable pressure mode was used, so carbon sputtering was not required. Several particularly suitable areas were selected for examination on each sample, i.e., where significant amounts of glaze or thicker drops of glaze adhered, which were marked prior to facilitating detection. The magnifications used in the examinations performed for this work ranged from 24× to 1156× magnification. Semiquantitative elemental analyses at the selected areas were performed using an energy-dispersive system (EDS).

Destructive Testing

Powder X-Ray Diffraction (XRD) and Micro-XRD (μ-XRD^2)

Glaze residue was removed from crucible rim fragment A45170048/8c with a scalpel, ground to powder with an agate mortar, and pressed onto a glass slide. The second sample was one of the lumps (A45170048/11f), from which the thick silvery-gray adherence was released with forceps and also ground to powder. XRD phase analysis of the two samples (A45170048/8c; A45170048/11f) was performed in the research laboratory of the Deutsches Bergbau-Museum in Bochum using a PANalytical X'Pert Pro X-ray powder diffractometer with a Cu x-ray source.

For a more detailed investigation of the microscopically observed crystals in the glaze of crucible rim fragment A45170048/8c, non-destructive and spatially resolved x-ray diffraction was performed at the CCA-BW in Tübingen directly on the exposed sections using a Bruker D8 Discover-GADDS micro-diffractometer equipped with a Co x-ray source and a large two-dimensional VÅNTEC-500 detector (μ-XRD^2) [21]. The beam diameter of the primary x-ray beam was approximately 80 μm using a 500 μm polycapillary X-ray optic. The PDF-2 database from ICDD (International Centre of Diffraction Data) was used for phase identification.

Lead Isotope Analysis

A portion of the galena sample (AKZ4518, 58:007) and glaze samples from two crucible rim fragments (A45170048/4 and A45170048/8b) were prepared for lead isotope analysis. For the two fragments, the material was obtained first by scraping off glaze residue from the surface with a scalpel; in addition, the very tightly adhering glaze was removed more successfully by using adhesive tape in combination with an excavator. Small sample quantities of 1–10 mg were sufficient for lead isotope analysis [22]. In an ultra-clean laboratory, the samples were dissolved in HF/HNO_3. Lead was separated based on a standardized protocol for the column chromatographic process [23]. This way, the lead was separated from the accompanying elements and concentrated. The lead solution was finally diluted to a 2% concentration of HNO_3. In the multi-collector mass spectrometer (Neptune Plus high-resolution MC-ICP-MS,

ThermoFisher Scientific), the prepared lead solution was then injected in a plasma.

The lead isotopes ^{204}Pb, ^{206}Pb, ^{207}Pb, and ^{208}Pb are separated in a magnetic field according to their mass. The advantage of a multi-collector device is that the isotopes of an element can be detected simultaneously. Tl standard is used for mass bias correction, and standard reference solution of NIST Pb 981 as an external standard. From the intensities obtained, lead isotope ratios are calculated. Lead isotope analysis is a common tool in archaeometry to discriminate and hence locate potential ore deposits. The lead isotope analysis of the fragments and the galena sample can be compared with lead deposits based on available reference ore data in the literature and databases [24, 25]. It must be noted at this point that the ores from which the reference data have been acquired were newly collected and are not identical to those actually mined in medieval times. It can be assumed that surface-near oxide ores were used first and that the sulfide ores were mined later. As far as it is known, the lead isotopy is not significantly different for oxidic and sulfide ores.

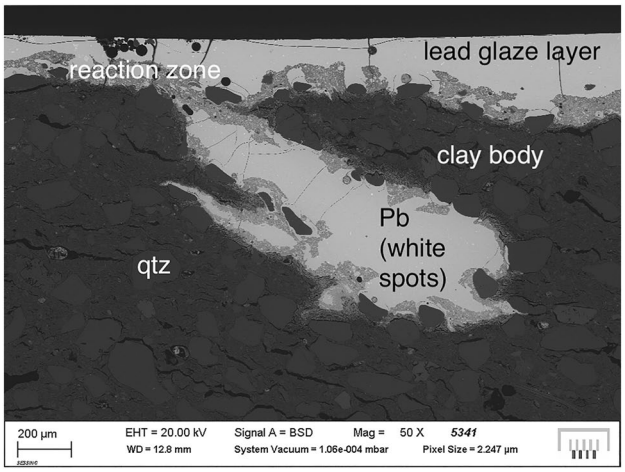

Fig. 4 Glaze layer and reaction zone between clay and glaze of sample A45170048_8b. The glaze is heterogeneous in composition and contains BSE white inclusions of lead. The clay has reacted and feeds the glaze with its components, while the quartz grains were not affected by the firing temperature

Results and Discussion

Macroscopically, all investigated fragments are red-colored and were hence fired under oxidizing environment as was previously proposed [13]. The glaze appears light to darker olive green to dark brown. The thickness of the glaze is heterogeneous, and in two examples (A45170048_11e and _11f), larger drips are attached to the fragments. Under polarized light microscopy, the substrate is a sub-microscopic clay with subangular quartz grains. The texture includes aligned shrinking cracks or such surrounding the quartz grains. The fragments reveal that they were pre-fired at rather low temperature, as one can observe a reaction zone between the clay body and the glaze layer. The reaction zone testifies to the fact that the clay fraction was melted here and chemically feeds the glaze, as one can see the material change in the backscattered SEM images, whereas quartz temper remained unchanged in shape and had not even partially melted (Fig. 4). The appearance meets in result of what also is known as common European medieval technique [26]: Lead ore or lead oxide was applied to the surface of the clay substrate, and under eutectic temperature, the glass ore obtains the required amount of silica from the clay. The German term is "Glasurerz-Rezept." The lead-rich eutectic temperature in the PbO-SiO_2 system is at 720 °C [27]. Angular to subangular relics of the ground galena ore in clay, glaze layer, or interface could be expected when considering this technique. In the Brilon samples, lead inclusions in the glaze are only observed as white globular spots in the microscale. Contrary to what is described for calcareous circumstances [28], the Brilon glazes are not significantly porous.

The glaze layer of crucible rim fragment A45170048/8c has an amorphous glassy structure and turned out to consist of a basic colorless glaze, in which a yellow phase had crystallized. Under the SEM in backscattered mode, different gray shades occur due to differences in the lead content of the glaze. The glaze layers are pervaded by cracks, and closed globular pores are observable. In one fragment, the glaze has intruded into the ceramic in molten state. The interface between the glaze and clay substrate appears as a reaction zone between both (Fig. 4). The glaze is heterogeneous in composition as can be seen in the BSE image.

Crystallized components in the amorphous glaze seem to always occur in chemical exchange with the glaze matrix: In darker gray areas, dark gray acicular crystals solidified, sometimes accumulated in sheaves. In lighter gray areas, white acicular crystals formed and are oriented along the interface between lighter and darker areas. Triangular crystals form clusters. Around clay fragments in the glaze layer, skeletal crystals had formed. Clay substrate and glaze have reacted as can be seen by a flow texture around the fragment. The different crystals observed are

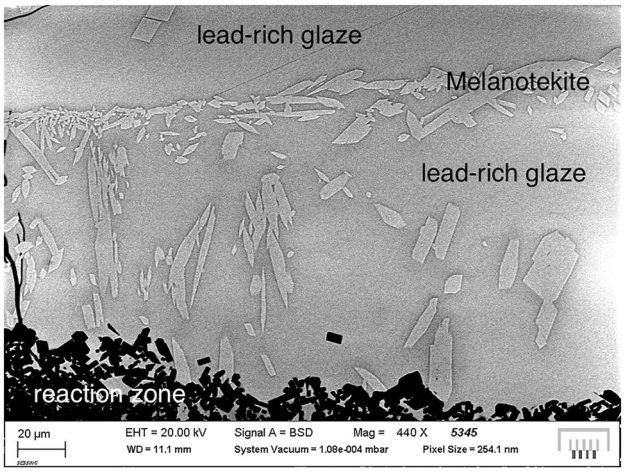

Fig. 5 Cooling history of the yellow crystals in the glaze layer of sample A45170048_11. Chill zone with tiny crystals (upper left), below this and in direction to the ceramic (bottom right): columnar grains

in total very small (< 100 µm) and, respectively, thin and could not be identified by the microscopical methods.

Greenish-yellow acicular crystals grow from the surface of the colorless glaze in direction of the clay substrate starting to crystallize along the surface of the glaze and develop toward the ceramic interface (samples A45170048_8b and A45170048_8c). Along the surface of the glaze, they form a solid crystal film. The strong thermal gradient between the rapidly cooling surface of the glaze and the slow-cooling clay substrate is responsible for the crystal film. The tiny crystals solidify in the surficial chill zone where the glaze remains as a melt and solidifies in an amorphous state later. Below the chill zone, the grains develop as columnar grains (Fig. 5). If they grow too large to resist the convection forces of the still molten glaze, they tear and disperse in the melt. What is noteworthy is that the chill zone results in a complete covering of the colorless glaze surface with a film of yellow crystals, which optically give the glaze a yellow to greenish color.

A rounded inclusion, around which crystals accumulate, cannot be clearly identified by the microscopic methods, but it appears to be a well-rounded fragment of clay. Colorless skeletal crystals stick out along the surface of the fragment. The glaze around the crystallized edge of the fragment is visibly brighter and has a flow texture (Fig. 6). It appears that the surrounding glaze offered components of its chemistry to the colorless crystals around the clay fragment. The crystals are extremely small and thin and hence cannot be analyzed without a compositional background of the glaze. However, comparable crystallization phenomena were previously presented in the literature. Reedy 2016 identified such needle-like crystals in comparable context as anorthite when interacting with the glaze. Wollastonite and hercynite were also mentioned, and cristobalite, the high-temperature modification of quartz, was described accordingly [29, 30]. By experimental work with a glazing mixture of $PbO + SiO_2$, Pb-rich feldspar crystals were produced in the diffusion zone of clay and glaze layer [31], and long firing and slow cooling resulted in more effective diffusion of elements resulting in a higher quantity of lead-potassium-rich feldspars. Diffusion of iron from the clay substrate to the glaze layer was also described [28]. Additionally, the incorporation of alumina and potassium was observed in the experiments. With XRD, we were able to identify only orthoclase, microcline, and

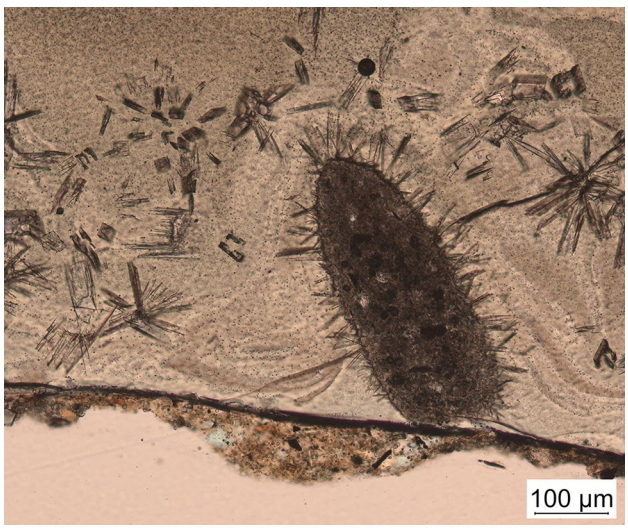

Fig. 6 Clay fragment in the glaze layer of sample A45170048_11. The glaze has changing chemistry around the clay fragment. Skeletal crystals form around the fragment, seemingly growing from the surface of the fragment into the still molten glaze

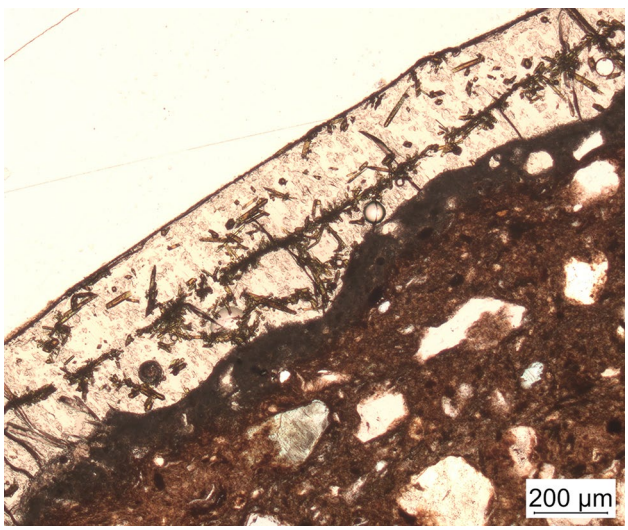

Fig. 7 Tandem glaze layer of sample A45170048_8 which is visibly separated by a film of yellow crystallization (S. Fischer-Lechner)

sanidine in samples A45170048-8 and 11. The richness of the composition of lead-silica crystallization in the diffusion zone as described in the literature [31] is not observable in the Brilon samples. This indicates rather fast cooling conditions so that the reaction partners have not had sufficient time to form the complex lead-potassium-alumina-rich phases.

Sample A45170048_8c shows a peculiarity; namely, a tandem layer of glaze was identified (Figs. 5 and 7). Two layers on top of each other were observed, on each of which the yellow crystals had formed from the chill zone of the surface of the glaze toward the ceramic (Fig. 7), which indicates fast cooling conditions of the glaze. This allows no other conclusion than the following sequence of solidification: The first glaze layer was allowed to cool and solidify: yellow crystals formed on the surface. Then, either intentionally or by chance, the process was repeated in the same way, so that the pottery was covered with a second glaze layer, on the surface of which again tiny yellow crystals were formed.

Scanning electron microscopy confirmed the visually observed structures and phases (Table 2). The amorphous glaze was analyzed in the different samples. Figure 8 visualizes the bulk composition and statistics based on the SEM analyses. The glaze produced on the investigated ceramic is a silica glass with 4.5–7.4 wt.% (first and third quartiles) alumina as a second component, and only minor amounts of potassium < 1.9 wt.% (third quartile), calcium < 0.7 wt.% (third quartile), magnesium < 0.4 wt.% (third quartile), and sodium < 0.4 wt.% (third quartile). Compared to the clay substrate, the glazes are not consistently enriched with silica (Fig. 9) and therefore do not correspond to the picture given for intentional glazes produced by applying $SiO_2 + PbO$ [32]. The lead addition to the silica glass is also rather random with 13.1–26.3 wt.% (first and third quartile) to 44. 9 wt.% at maximum (Fig. 10) and does not meet the transparent high lead glazes from Europe and the Near East spanning the period from the third to eighteenth century CE [33]. Iron content ranges between 2.4 and 3.5 wt.% (first and third quartiles), which contributes substantially to the green to brown color of the glazes.

The gray and skeletal crystals were analyzed, and they were found to contain less lead than the amorphous glaze. It remained difficult to identify them, because they are even too small and thin for the SEM and hence are not really distinguished significantly from the composition of the amorphous glaze. Presumably, the gray crystals are crystallized lead-silica phases, which grew from the glaze melt, while it cooled down. Furthermore, the yellow crystals forming on the surfaces could not be identified by elemental analysis in the energy-dispersive SEM. The analysis was not conclusive, once detecting arsenic and sulfur, but not in other regions. The post-Variscan galena from Brilon was described as being nearly arsenic-free (< 10 ppm, Atomic Absorption Spectrometry; Schaeffer 1984). As mentioned earlier, arsenic and lead overlap in the energy spectrum. Since lead is present in high amounts in the samples, arsenic has been considered a fragment in the spectrum. Because the measurements yielded iron content, the guess was hematite. However, the crystal shape of the observed yellow crystals is contradictory to the crystallography of trigonal hematite.

For this reason, a powder XRD (XRPD) was performed on the powders of glazes adhering to two fragments. The thermal phase (trans-)formation of glazes in the PbS-SiO_2 system was investigated previously by high-temperature resolved XRD and the phase diagram was investigated [34]. In the glaze layer of fragment A45170048/8b, the crystallized components quartz, orthoclase, hematite and lead (Pb) were identified; in the glaze layer of fragment A45170048/11f, sanidine and lead (Pb) were identified. No evidence was found for phase identification of the yellow acicular crystals. Therefore, µ-XRD analysis was performed at the CCA-BW in Tübingen to identify the yellow crystals directly in noncovered cross-sections. In this way, melanotekite, a synthetic orthorhombic sorosilicate ($Pb_2Fe_2^{3+}(Si_2O_7)O_2$) could be identified (Fig. 11). Melanotekite was reported earlier in lead glaze-related publications, and its phase relation to hematite and consequences for the reconstruction of melting temperatures were discussed [32, 35]. It can result in yellow to brown decorations, e.g., of seventeenth-/nineteenth-century CE ceramic lead glaze [30]. Reviewing the powder diffractograms for this phase finally delivered the complete picture of crystallized phases as present in the glaze layers (Table 3). Hematite is in no case co-existent with melanotekite here. Since melanotekite dissolves completely at firing temperatures above 920 °C (following Di Febo et al.'s arguments [35]), from which during cooling it can form the observed skeletal yellow crystals, the presence of the phase in absence of hematite indicates rather high melting temperatures to produce the glazes adhering on the lumps from Brilon.

To position the glaze layers into the metallurgical context of the region, the galena sample and two samples of the glaze have been analyzed for lead isotope composition (Table 4). The lead isotope signature of the glaze is dominated by the lead component, so that the glazes could be compared with the lead ores of the region. Reference data of lead ores from the Brilon region are provided in the dissertation of M. Bode [9]. While the two glaze samples show

Table 2 EDS–SEM analysis of the glaze layer, crystallized phases and ceramic body in the analyzed samples

Object	Component	O	Na	Mg	Al	Si	P	S	K	Ca	Ti	Fe	Cu	As	Pb
		weight percentage, normalized to 100%													
Glaze layer															
A45170048/11b	Amorphous glass	46.6	0.0	0.7	5.2	31.0	0.0	0.0	1.0	1.1	0.0	3.4	0.0	0.0	11.0
A45170048/11b	Amorphous glass	47.5	0.0	0.9	5.8	27.5	0.0	0.0	1.1	1.3	0.0	3.7	0.0	0.0	12.2
A45170048/11b	Amorphous glass	47.4	0.0	0.8	6.1	26.7	0.0	0.0	1.3	0.9	0.0	3.1	1.5	0.1	12.0
A45170048/11b	Amorphous glass	33.9	0.0	0.5	4.7	26.1	0.0	0.0	0.9	0.7	0.0	3.1	1.5	12.4	16.2
A45170048/11b	Amorphous glass	37.3	0.0	0.5	4.5	24.3	0.0	0.0	0.7	0.7	0.4	2.3	1.0	9.9	18.5
A45170048/11b	Amorphous glass	38.8	0.0	0.6	4.8	19.7	0.0	0.0	0.8	0.5	0.0	3.0	0.0	0.0	31.8
A45170048/11b	Amorphous glass	33.6	0.4	0.3	4.6	24.6	0.0	0.0	1.0	0.6	0.0	2.4	1.7	10.5	20.3
A45170048/11b	Amorphous glass	34.1	0.0	0.4	5.5	26.8	0.0	0.0	1.0	0.0	0.4	2.0	1.5	15.5	13.1
A45170048/11b	Amorphous glass	34.2	0.0	0.4	4.3	22.2	0.0	0.0	0.8	0.6	0.0	2.5	1.9	0.0	33.0
A45170048/11b	Amorphous glass	39.6	0.0	0.0	4.1	25.9	0.0	0.0	1.2	0.8	0.0	0.0	2.4	0.2	25.6
A45170048/11b	Amorphous glass	38.2	0.0	0.0	4.5	25.6	0.0	0.0	1.1	0.4	0.0	3.0	2.0	0.1	25.1
A45170048/11b	Amorphous glass	39.1	0.4	0.0	4.9	27.9	0.0	0.0	1.2	0.7	0.0	3.8	1.9	0.7	19.4
A45170048/11d	Amorphous glass	39.1	0.0	0.0	7.4	27.9	0.0	0.0	2.2	0.0	0.0	3.5	1.5	0.5	17.9
A45170048/11b	Transition zone	47.0	0.4	0.5	9.8	27.9	0.0	0.0	5.4	0.0	0.0	2.2	0.0	0.0	6.8
A45170048/11d	Amorphous glass	43.5	0.2	0.0	7.7	31.6	0.0	0.0	3.5	0.6	0.0	3.6	0.0	0.3	9.0
A45170048/11d	Amorphous glass	41.9	0.4	0.0	7.4	29.9	0.0	0.0	3.4	0.0	0.0	2.9	0.0	0.5	13.6
A45170048/11d	Amorphous glass	37.1	0.0	0.0	9.4	23.7	0.0	0.0	1.8	0.0	0.0	2.7	0.0	0.5	24.8
A45170048/11d	Amorphous glass	33.9	0.0	0.5	12.5	25.5	0.0	0.0	1.3	0.0	0.0	3.3	0.0	9.3	13.8
A45170048/11d	Amorphous glass	29.4	0.0	0.0	12.5	23.3	0.0	0.0	1.1	0.0	0.5	2.4	0.0	14.4	16.5
A45170048/11e	Amorphous glass	33.6	0.0	0.0	5.3	13.8	0.0	0.0	1.9	0.0	0.0	3.1	0.0	0.0	42.4
A45170048/11e	Amorphous glass	37.3	0.0	0.4	4.5	21.9	0.8	0.0	1.3	1.4	0.0	3.8	1.8	0.2	26.5
A45170048/11e	Amorphous glass	38.9	0.6	0.6	4.4	20.5	0.0	0.0	1.4	0.6	0.4	2.6	1.9	0.0	28.0
A45170048/11f	Amorphous glass	40.3	0.0	0.6	4.8	26.1	0.0	0.0	1.4	0.7	0.7	3.0	0.0	0.0	22.5
A45170048/11f	Amorphous glass	45.6	0.0	0.7	5.8	31.1	0.0	0.0	1.7	1.0	0.0	3.8	0.0	0.0	10.4
A45170048/11f	Amorphous glass	49.1	0.5	0.0	6.7	28.5	0.0	0.0	2.2	1.1	0.5	3.1	0.0	0.5	7.9
A45170048/11f	Amorphous glass	44.6	0.4	0.0	5.3	24.4	0.0	0.0	1.5	1.3	0.0	4.0	0.0	0.0	18.5
A45170048/11f	Amorphous glass	46.5	0.1	0.0	6.0	32.3	0.0	0.0	1.3	1.2	0.0	3.8	0.0	0.4	8.4
A45170048/11f	Amorphous glass	29.3	0.0	0.6	3.3	17.6	0.0	0.0	0.8	0.8	0.0	2.7	0.0	0.0	44.9
A45170048/11f	Clay fragment bright area	40.3	0.0	0.8	4.4	25.6	0.0	0.0	1.1	0.9	0.6	2.9	0.0	0.0	23.4
A45170048/11f	Clay fragment bright area	46.1	0.0	0.7	5.6	29.6	0.0	0.0	1.5	0.9	0.7	4.3	0.0	0.1	10.4
A45170048/11f	Clay fragment dark area	46.7	1.0	0.0	11.3	27.8	0.0	0.0	6.7	0.0	0.0	1.6	0.0	0.0	4.9
A45170048/11f	Clay fragment dark area	43.9	0.7	0.6	13.6	24.4	0.0	0.0	3.7	0.7	0.0	7.1	0.0	0.0	5.4
A45170048/11f	Clay fragment dark area	46.1	0.9	0.0	10.0	28.1	0.0	0.0	8.3	0.0	0.0	1.3	0.0	0.0	5.5
A45170048/11f	Skeleton crystal	45.3	0.6	0.2	8.8	28.2	0.0	0.0	8.5	0.0	0.0	1.4	0.0	0.0	6.9
A45170048/4	Acicular crystal	37.0	0.0	0.5	4.7	15.6	0.0	0.0	0.6	0.0	1.3	13.3	0.0	0.0	26.9
A45170048/4	Amorphous glass	37.2	0.2	0.3	5.6	18.4	0.0	0.0	0.7	0.0	0.6	3.5	0.0	0.0	33.3
A45170048/4	Amorphous glass	37.0	0.0	0.4	5.7	20.9	0.0	0.0	0.7	0.0	0.0	4.3	0.0	0.0	30.9
A45170048/8b	Amorphous glass	34.0	0.0	0.0	3.5	20.8	0.0	0.0	0.7	0.0	0.4	1.8	0.0	0.0	38.8
A45170048/8b	Amorphous glass	38.1	0.0	0.4	4.6	25.8	0.0	0.0	0.7	0.0	0.0	1.2	0.0	0.0	29.3
A45170048/8b	Amorphous glass	9.2	0.0	0.0	8.3	49.2	0.0	0.0	0.0	0.0	0.0	4.6	0.0	0.5	28.2
A45170048/8b	Amorphous glass	41.7	0.4	0.0	4.0	25.4	0.0	0.0	1.1	0.0	0.4	2.5	0.0	12.4	12.1
A45170048/8b	Amorphous glass	41.3	0.4	0.0	3.6	23.4	0.0	0.0	1.2	0.0	0.0	1.5	0.0	0.2	28.3
A45170048/8b	Amorphous glass	44.4	0.6	0.0	4.0	27.1	0.0	0.0	1.2	0.0	0.0	3.4	0.0	0.6	18.7
A45170048/8b	Amorphous glass	46.2	0.4	0.0	4.0	27.5	0.0	0.0	1.4	0.5	0.5	2.8	0.0	0.3	16.5
A45170048/8b	Amorphous glass	47.8	0.7	0.0	4.2	29.1	0.0	0.0	1.4	0.0	0.0	2.9	0.0	0.5	13.3
A45170048/8b	Antimony triangular pyramid	45.8	0.0	0.0	3.8	14.2	0.0	0.0	1.0	0.0	3.1	7.9	0.0	0.0	24.1
A45170048/8b	Transition zone	45.9	0.5	0.4	9.7	27.9	0.0	0.0	4.3	0.0	0.0	1.9	0.0	0.0	9.4
A45170048/8b	Transition zone	47.9	0.6	0.2	10.1	28.4	0.0	0.0	4.0	0.0	0.0	1.7	0.0	0.0	7.2

Table 2 (continued)

Object	Component	O	Na	Mg	Al	Si	P	S	K	Ca	Ti	Fe	Cu	As	Pb
		weight percentage, normalized to 100%													
A45170048/8c	Acicular crystal	33.9	3.1	0.0	0.0	15.9	0.0	0.0	0.0	0.0	1.1	17.6	0.0	0.0	28.5
A45170048/8c	Acicular crystal	36.7	0.0	0.6	7.1	21.7	0.0	0.0	0.0	0.0	0.0	19.4	0.0	0.0	14.6
A45170048/8c	Acicular crystal	37.2	0.0	0.0	6.5	20.1	0.0	0.0	0.0	0.0	1.1	18.6	0.0	1.0	15.4
A45170048/8c	Acicular yellow crystal	47.5	0.0	0.8	3.2	20.5	0.0	0.0	0.8	0.0	1.0	16.7	0.0	0.0	9.5
A45170048/8c	Acicular yellow crystal	38.9	0.0	0.2	3.1	18.8	0.0	0.0	0.0	0.0	1.0	22.7	0.0	0.0	15.3
A45170048/8c	Acicular yellow crystal	34.1	0.0	0.3	2.4	15.0	0.0	0.0	0.0	0.0	0.8	18.8	0.0	0.0	28.6
A45170048/8c	Acicular yellow crystal	43.7	0.0	0.3	3.7	20.4	0.0	0.0	0.8	0.0	0.7	22.7	0.0	0.0	7.7
A45170048/8c	Acicular yellow crystal	41.5	0.0	0.0	3.5	20.6	0.0	0.0	0.0	0.0	0.0	23.8	0.2	0.0	10.4
A45170048/8c	Amorphous glass	49.7	0.0	0.7	6.1	29.3	0.0	0.0	0.7	1.7	0.0	3.7	0.0	0.2	7.9
A45170048/8c	Amorphous glass	31.4	0.0	36.9	3.8	18.8	0.0	0.0	0.6	0.9	0.0	1.9	0.0	0.1	5.7
A45170048/8c	Amorphous glass	43.4	0.0	0.5	6.5	27.1	0.0	0.0	0.9	0.0	0.0	2.9	0.0	0.0	18.6
A45170048/8c	Amorphous glass	37.8	0.0	0.4	4.9	22.5	0.0	0.0	0.6	0.0	0.0	2.3	0.0	0.0	31.5
A45170048/8c	Amorphous glass	46.1	0.0	0.5	7.1	26.0	0.0	0.0	0.8	0.6	0.0	3.9	0.0	0.0	15.0
A45170048/8c	Transition zone	48.4	0.7	0.4	10.8	27.3	0.0	0.0	4.4	0.0	0.0	1.7	0.0	0.0	6.3
A45170048/8c	Transition zone	42.4	0.0	0.6	5.2	26.5	0.0	0.0	0.8	0.9	0.0	3.2	0.0	0.0	20.3
A45170048/8c	Transition zone	48.0	0.8	0.0	13.1	26.8	0.0	0.0	4.4	0.0	0.0	1.1	0.0	0.0	5.8
A45170048/8d	Acicular crystal	48.9	0.4	0.0	7.1	30.4	0.0	0.0	4.4	0.0	0.0	1.2	0.0	0.0	7.5
A45170048/8d	Acicular crystal	44.7	0.5	0.0	11.3	29.2	0.0	0.0	7.9	0.0	0.0	1.3	0.0	2.0	3.0
A45170048/8d	Acicular crystal	48.4	0.0	0.3	8.0	31.5	0.0	0.0	5.2	0.0	0.0	1.5	0.0	0.0	5.1
A45170048/8d	Acicular crystal	48.2	0.4	0.0	8.7	31.1	0.0	0.0	6.5	0.0	0.0	1.3	0.0	0.4	3.5
A45170048/8d	Acicular crystal	45.6	0.7	0.4	11.1	23.4	0.3	0.0	6.0	0.0	0.0	2.7	0.0	0.0	9.8
A45170048/8d	Amorphous glass	47.3	0.2	0.0	8.1	28.4	0.0	0.0	4.2	0.0	0.0	0.8	0.0	0.0	11.1
A45170048/8d	Amorphous glass	46.4	0.4	0.0	9.4	30.0	0.0	0.0	3.8	0.0	0.0	1.9	0.0	0.1	8.0
A45170048/8d	Amorphous glass	43.1	0.0	0.0	10.0	30.0	0.0	0.0	2.4	0.6	0.0	3.3	0.0	0.6	10.0
A45170048/8d	Amorphous glass	47.7	0.0	0.0	9.0	31.6	0.0	0.0	4.1	0.0	0.0	2.1	0.0	0.2	5.3
AKZ4518	Galena	0.0	0.0	0.0	0.0	0.0	0.0	38.1	0.0	0.0	0.0	0.0	0.0	0.0	61.9
AKZ4518	Galena	0.0	0.0	0.0	0.0	0.0	0.0	35.8	0.0	0.0	0.0	0.0	0.0	0.0	64.2
AKZ4518	Galena	29.9	0.0	0.0	0.0	0.0	0.0	25.2	0.0	0.0	0.0	0.0	0.0	0.0	44.8
AKZ4518	Galena	34.3	0.0	0.0	0.3	0.0	0.0	25.0	0.0	0.0	0.0	0.0	0.0	0.0	40.4
AKZ4518	Galena	0.0	0.0	0.0	0.4	0.0	0.0	35.2	0.0	0.0	0.0	0.0	0.0	0.0	64.4
Clay body															
A45170048/4		46.0	0.2	0.7	14.6	22.8	0.9	0.9	3.4	0.0	1.0	9.6	0.0	0.0	0.0
A45170048/4		42.8	0.0	0.7	16.6	22.7	1.3	2.0	4.1	0.0	0.4	9.5	0.0	0.0	0.0
A45170048/8d	Small area surrounded by glazing	50.4	0.2	1.2	21.0	16.9	0.0	0.0	2.0	0.5	0.5	4.3	0.0	0.0	2.9
A45170048/11b		67.4	0.0	1.0	4.9	10.1	0.0	0.0	2.9	0.0	0.0	13.7	0.0	0.0	0.0
A45170048/11d	Close to glazing	57.9	0.0	0.2	1.9	35.6	0.0	0.1	0.5	0.0	0.4	2.0	0.0	0.0	1.4
A45170048/11d	Close to glazing	46.8	0.0	0.0	9.2	20.0	4.6	0.0	0.8	0.5	0.9	14.6	0.0	2.7	0.0
A45170048/11d	Small area surrounded by glazing	49.5	0.3	0.0	13.0	19.0	1.7	0.0	2.3	3.6	0.3	8.5	0.0	1.7	0.0
A45170048/11e		52.4	0.0	0.4	4.2	39.9	0.0	0.6	0.6	0.0	0.0	2.0	0.0	0.0	0.0
A45170048/11e		57.5	0.3	0.5	6.0	32.7	0.0	0.0	1.0	0.0	0.0	1.6	0.0	0.0	0.4
A45170048/11f		51.3	0.9	0.6	11.0	26.4	0.6	0.8	3.9	0.0	0.5	4.1	0.0	0.0	0.0
A45170048/11f	Small area surrounded by glazing	52.6	0.4	0.0	11.7	25.1	0.3	0.0	2.7	0.6	0.4	4.0	0.0	1.5	0.7

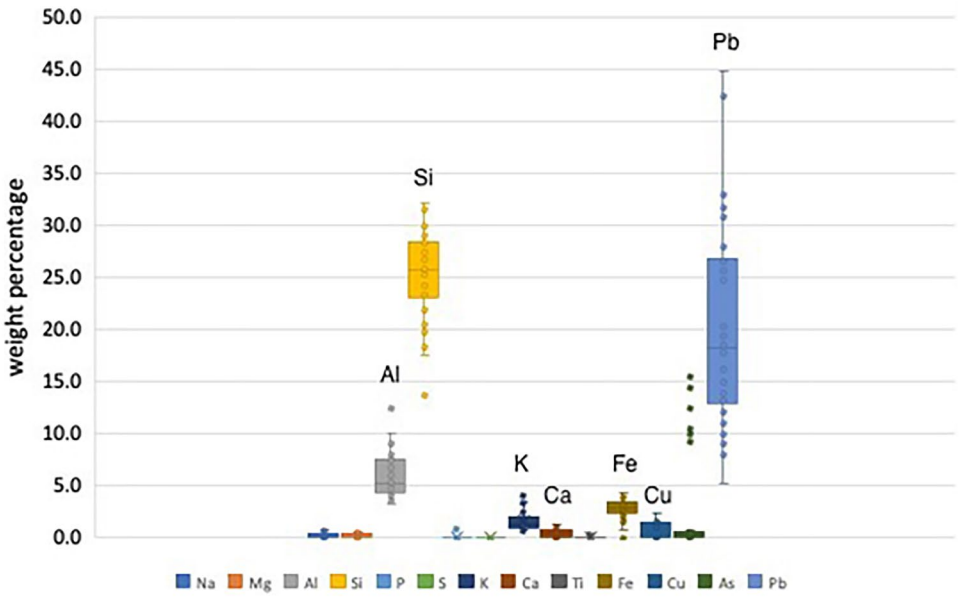

Fig. 8 Box–Whisker plot for the glaze composition. The glaze composition follows a recipe of an alumina-silica glass with 4.3–7.5 wt. Al (values in the box = quartiles 1–3) and variable and heterogeneous lead content between 9.2 and 22.2 wt.% Pb (values in the box = quartiles 1–3)

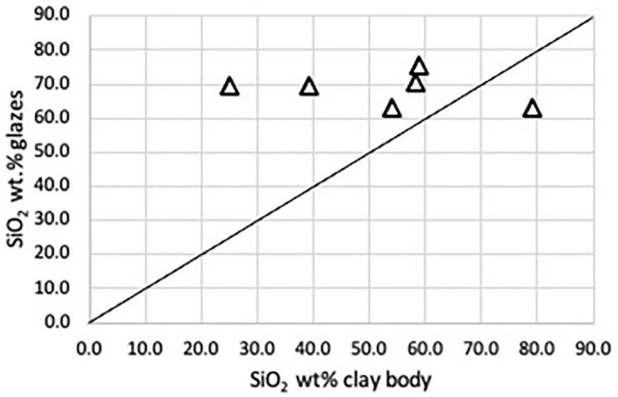

Fig. 9 Comparison of SiO_2 concentration in weight percentage in glaze layer and ceramic body. SiO_2 in the glaze layer is elevated, but rather random

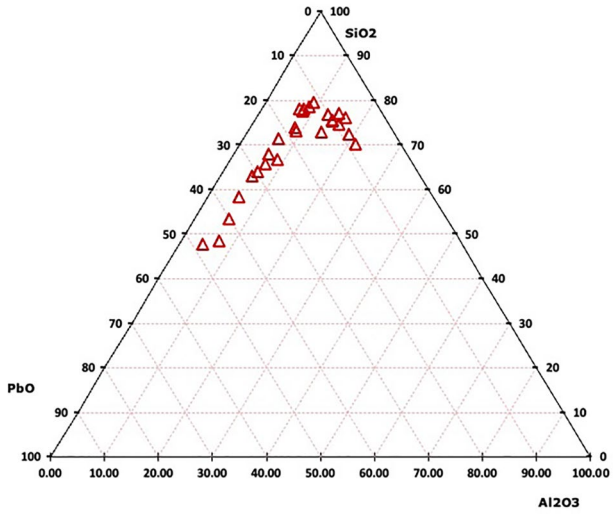

Fig. 10 Ternary diagram SiO_2-Al_2O_3-PbO of analyzed glaze composition. Lead content is rather random

an identical Pb isotope signature within the error limits, the galena sample contains higher radiogenic lead (Fig. 12). The galena sample and the glazes fit well into the overall picture of the Brilon anticline. With a closer look into the reference data, however, two isotope fields can be developed which distinguish the eastern and the western part of the anticline (Fig. 12). Higher radiogenic lead represents the eastern part (Alme, Bleiwäsche, Madfeld, Messinghausen, Rösenbeck), and lower radiogenic lead characterizes the western part (Brilon and surroundings). The examined galena sample matches a high medieval lead mine in the Buchholz Forest in the eastern part. According to finds in the surrounding area, it can be dated to the tenth–eleventh century, thus even slightly older than the excavated pottery kiln. As expected, the analyzed galena sample perfectly matches the ore reference data from the eastern part of the Brilon anticline. The glazed fragments originating from the Lühlingsbach valley in the eastern part were found in close proximity (less than 2 km away) to the site of the galena sample. Surprisingly, their lead isotope signature is clearly different and rather fits the reference data of the western part. The best match is actually with samples from Kirchloh hill 3 km southeast of Brilon. It must

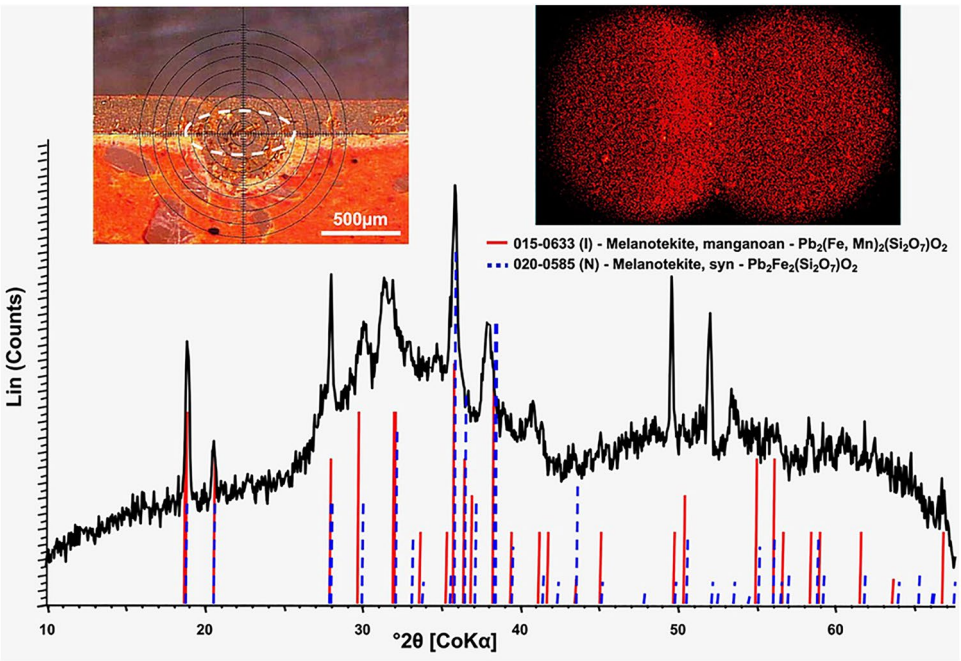

Fig. 11 Image of the measurement location (white ellipse) of the µ-XRD^2 measurement in an area with yellow acicular crystals in the glaze (left), detector images of the measurement with single-crystal spots (right) and resulting diffractogram with reference patterns of melanotektite from the PDF-2 database (bottom) which is in good accordance with the measured pattern. It is important to note that the measured intensities are strongly influenced by the single-crystal intensities which are visible in the detector images. Therefore, they will not necessarily correlate with the theoretical intensities from the database. The hump in the diffractogram results from the amorphous matrix (glass) of the glaze. Measurement time for each detector image was 10 min. Sample A45170048_8

be emphasized here, however, that [9] reference data were not compiled with an eye to the fact that the mines were also operated during the period in question. Further investigation in the former Brilon mining district is needed to clarify this.

Conclusions

Glazes represent the earliest examples of the production of glass. Observations related to pyrometallurgical processes have shown that glazes can be produced even unintentionally in the smelting furnace. The site of this study is a further example of a strong relationship between metallurgy and glaze production. The region is very rich in lead ore. There is a large number of pits in the area, and metallurgical activity in the region is evident. Pottery production took place and has been evidenced by the excavation of a pottery kiln. Inside the kiln, the latest furnace journey has been preserved. The kiln was loaded with unglazed pottery. Remains which would point to glazing activities such as crushed lead ore, litharge, quartz, crucibles, grinding tools, or other pigments were not found. The investigated fragments, which are thick-walled, coarse-grained fragments of crucibles and furnace walls, were found in a nearby waste dump together with finely produced and glazed pottery products. Archaeological evidence hence suggests that the dump was at least partially filled with metallurgical waste from the pits and not solely with glazed pottery. It remains unproven whether the glaze production took place on-site or remotely.

There are many requirements such as chemistry, components, or temperatures for the successful production of pottery glazes. As archaeological examples demonstrate, the metallurgical context fulfills the same physicochemical reactions then often described as slagging or vitrification: a random silica melt from silica-rich clay enriched with the endemic metal (e.g., Cu, Fe, Pb): Due to the high

Table 3 Phases identified by XRPD and µ-XRD^2

	Sample nb	
	A45170048_8c	A45170048_11f
SiO_2, quartz low	x	
$Pb_2Fe_2(Si_2O_7)O_2$, syn. melanotekite	x	
$Al_1K_1O_8Si_3$, microcline	x	
$KAlSi_3O_8$, sanidine		x
Pb_1, lead	x	x
Fe_2O_3, hematite	x	
$Al_1K_1O_8Si_3$, orthoclase	x	

Table 4 Lead isotope results of the lead glazes and the galena sample

Sample nb		206Pb/204Pb	2SD	2SE	207Pb/204Pb	2SD	2SE	208Pb/204Pb	2SD	2SE	207Pb/206Pb	2SD	2SE	208Pb/206Pb	2SD	2SE
AKZ 4518,58:007	Galena	18.4500	0.0027	0.0004	15.6187	0.0033	0.0005	38.4062	0.0085	0.0014	0.8466	0.0001	0.0000	2.0815	0.0002	0.0000
A 4517_0048/8b	Glaze	18.3450	0.0026	0.0004	15.6111	0.0029	0.0005	38.2752	0.0072	0.0012	0.8510	0.0001	0.0000	2.0863	0.0001	0.0000
A 4517_0048/4	Glaze	18.3464	0.0027	0.0004	15.6110	0.0026	0.0004	38.2761	0.0061	0.0010	0.8510	0.0000	0.0000	2.0862	0.0001	0.0000
Monitoring		206Pb/204Pb			207Pb/204Pb			208Pb/204Pb			207Pb/206Pb			208Pb/206Pb		
NIST SRM 981, n = 7 (2σ)		16.9307 (±6)			15.4843 (±6)			36.6752 (±16)			0.914567 (±10)			2.16619 (±4)		
Samples normalized to		16.9306			15.4834			36.6749			0.9146			2.1661		

The NIST SRM 981 standard reference material was measured as unknown sample for internal monitoring

temperatures in pyrometallurgical furnaces, the lining, technical ceramic, or tuyère tips can be partially melted. The color spectrum is also equally attainable, so that red, green, yellow, brown, or black glazes can be formed due to metal vapors. Neo-crystallized phases (feldspars, SiO_2 modifications [16]) also form similarly during the cooling processes. The glassy layers found on the investigated fragments were identified as amorphous Al-Si-Pb glass with low concentrations of Na, Ca, K, Mg, and K. They are of a fairly heterogeneous yellowish-green to brown color. The silica and lead concentrations are quite variable and apparently do not follow a consistent mixture. The pottery was not well prepared, as one would expect a smoothing of the surface to produce high quality and glossy glaze on pottery (e.g., in Renaissance pottery [36]). In some cases, glassy drips can be observed, showing that the glaze was quite viscous at times. The glaze exhibits numerous cracks, which may indicate differential shrinkage relative to the clay substrate. It is to be expected that the cracking would have been avoided in deliberate production. The presence of identified melanotekite and its specific behavior in the melt is indicative of fairly high furnace temperatures and other lead-silica phases usually observed from neo-crystallization in the reaction zone between the clay body and glaze are absent. The coloration is not homogeneous throughout the glaze layer, as it is expected if ferrous glazes overlay the original clay color. Rather, when the yellow idiomorphic melanotekite crystals have formed they are concentrated in the chill zone of the glaze and are not distributed throughout. This results in a thin, yellow-to-green film and makes the glaze, which is colorless in itself, appear yellow to green when observed by the naked eye. The tandem layer, as observed on one of the samples and never before, does not meet a professional glazing process. The molten mass seems to have overflowed several times rather accidentally.

To summarize, the substantial chemical reactions and occurring phases observed here were previously characterized in the context of lead glazing techniques. However, they are also consistent with what is known in a metallurgical and hence non-intentional context. The use of glazed products in the region is supported by the finds in the excavation, but the lack of evidence for glaze production in the immediate vicinity leaves the question open of whether or not pottery activities included glazing on site. It is evident that pottery production and metallurgical activities were closely related in the region. Lead isotope analysis has shown that the fact that the ore is available right on the doorstep does not mean that it was used exclusively. Apparently, lead ore was collected and used throughout the region, regardless of whether it came from the western or eastern part of the Brilon anticline.

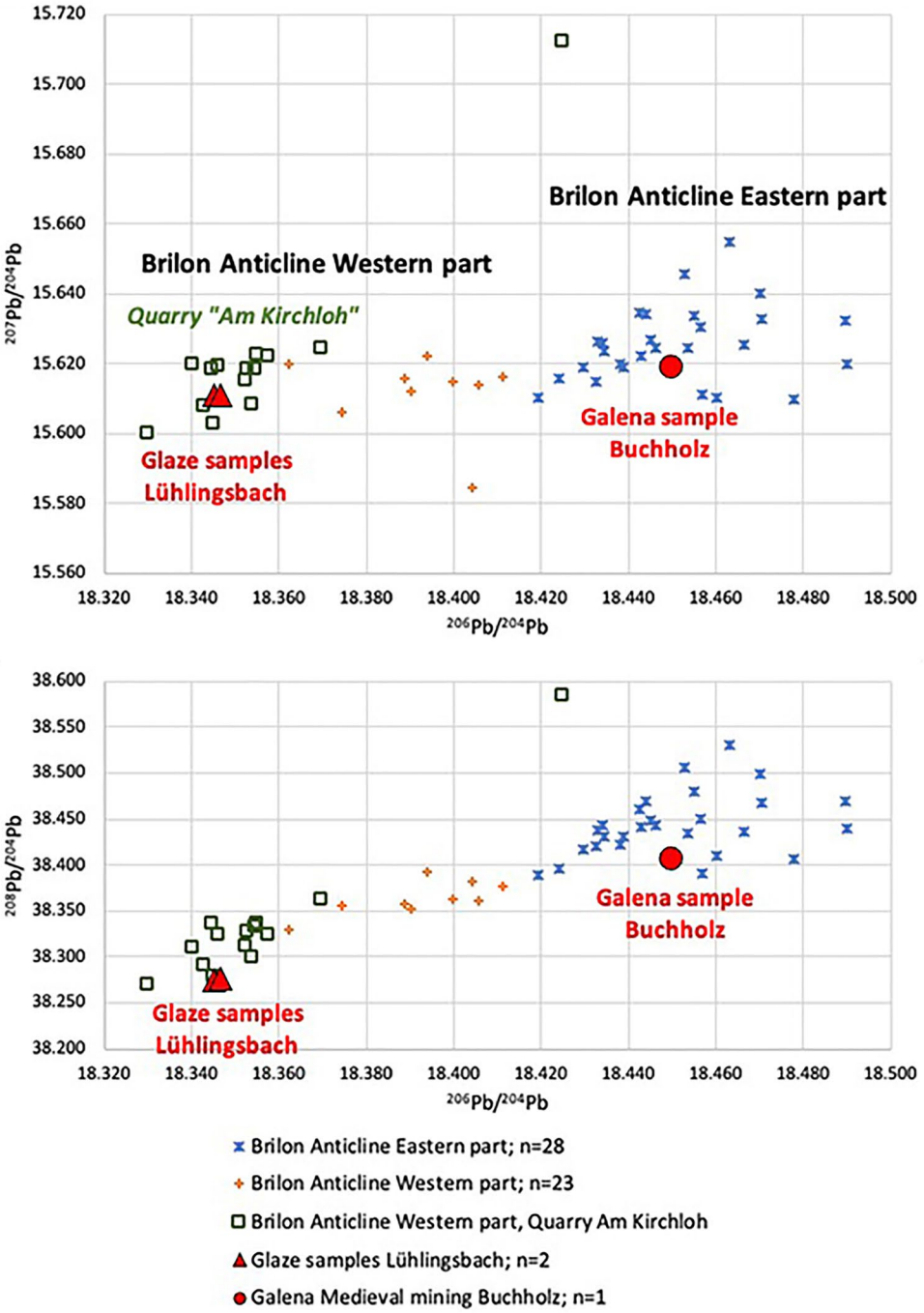

Fig. 12 Lead isotope diagrams comparing the own samples (glazes, galena sample from Buchholz) and 51 reference data for the Brilon anticline from the literature [9]

Acknowledgements We are grateful to have received the fragments for analysis by the LWL—Landschaftsverband Westfalen-Lippe. The elemental and isotope analyses were run in the research laboratory of the Deutsches Bergbau-Museum Bochum. Our thank goes to Dr. Moritz Jansen for the lead isotope analyses, Sandra Kruse genannt Lüttgen for the thin section preparation, and the technical staff of the laboratory for much help. At the LWL, we would like to thank Maja Thede for the geographic part of the map and Hannah Zietsch from the Deutsches Bergbau-Museum/Archaeometallurgy for the geological redrawing. At the Competence Center Archaeometry—Baden-Wuerttemberg (CCA-BW), Beatrice Boese is especially thanked for running the μ-XRD^2 measurements. We would like to thank Nadine Svane und Jana Klepacova for English proofreading. We acknowledge the helpful comments of the anonymous reviewers and the help of the editor, based on which we were able to improve our final manuscript.

Funding Open Access funding enabled and organized by Projekt DEAL.

References

1. R.D. Dallmeyer, W. Franke, K. Weber, *Pre-Permian Geology of Central and Eastern Europe* (Springer Verlag, Berlin, Heidelberg, 1995)
2. P. Bär, *Stratigraphie, Fazies und Tektonik am Briloner Massenkalk-Sattel (Ostsauerland)* (Justus-Liebig-Universität Gießen, Gießen, 1966)
3. Y. Wahba, *Die Geologie des Briloner Massenkalksattels im Östlichen Sauerland* (TU Clausthal, Clausthal, 1987)
4. A. May, Der Massenkalk (Devon) nördlich von Brilon (Sauerland). Geol. Paläontol. Westfal. **10**, 51–84 (1987)
5. W. Schriel, Der Briloner Galmei-Distrikt. Z. Dtsch. Geol. Ges. **106**, 308–349 (1956)
6. R. Schaeffer, *Die Postvariszische Mineralisation im Nordöstlichen Rheinischen Schiefergebirge*. Ph.D. Thesis, Available from Technische Universität Braunschweig, Braunschweig, Germany. Thesis completed (1984)
7. M. Bonhomme, D. Bühmann, Y. Besnus, Reliability of K-Ar dating of clays and silifications associated with vein mineralizations in western Europe. Geol. Rundsch. **72**, 105–117 (1983)
8. T. Kirnbauer, T. Wagner, H. Taubald, M. Bode, Post-Variscan hydrothermal mineralization, Taunus, Rhenish Massif (Germany): constraints from stable and radiogenic isotope data. Ore Geol. Rev. **48**, 239–257 (2012)
9. M. Bode, *Archäometallurgische Untersuchungen zur Blei-/Silbergewinnung im Germanien der Frühen Römischen Kaiserzeit*. Ph.D. Thesis, Available from Westfälische Wilhelms-Universität Münster, Münster, Germany. Thesis completed (2008)
10. Kgl. Oberbergamt Bonn, *Beschreibung der Bergreviere Arnsberg*. Brilon und Olpe sowie der Fürstenthümer Waldeck und Pyrmont (1890)
11. N. Hanel, P. Rothenhöfer, W. Melzer, Römische Bleigewinnung im Raum Brilon und der Bleitransport nach Rom. In *Bleibergbau und Bleiverarbeitung während der römischen Kaiserzeit im rechtsrheinischen Barbaricum, Soest*, ed. by T. Capelle (Westfälische Verlagsbuchhandlung Mocker & Jahn, 2007)
12. M. Zeiler, Feuer-Wasser-Erz: Die Gewinnung von Metallen im Mittelalter. In *Echt Alt! Mittelalterliches Handwerk Ausgraben*, ed. by L. Westfalen-Lippe (2018), pp. 100–113
13. W. Essling-Wintzer, R. Bergmann, E. Cichy, Der Töpferofen von Brilon-Alme. *Archäologie in Westfalen-Lippe* (2016), pp. 98–103. https://doi.org/10.11588/AIW.2015.0.33890
14. R. Köhne, W. Reininghaus, *Berg-, Hütten- und Hammerwerke im Herzogtum Westfalen im Mittelalter und in der Frühen Neuzeit* (Aschendorff, Münster, 2008)
15. M. Zeiler, Archäologie mit Sprengstoff: Archäologische Untersuchung eines Pingenzugs bei Brilon. *Archäologie in Westfalen-Lippe* (2020), pp. 132–135. https://doi.org/10.11588/AIW.2020.84262
16. A. Hauptmann, S. Klein, Über die Bildung von Glasuren in alten Kupferschmelzöfen. In *Türkis und Azur – Quarzkeramik im Orient und Okzident*, ed. by R. Busz, P. Gercke (Edition Minerva, 1999), pp. 114–120
17. P.R.S. Moorey, *Ancient Mesopotamian Materials and Industries* (Clarendon Press, Oxford, 1994)
18. S. Klein, F. Zereini, H. Urban, M. Schuster, K.-H. König, Die Edelmetalle – Anreicherung, Selektion und Nachweis. In *Forschung, Entwicklung, Projekte – Messe-Exponate der Uni Frankfurt*, ed. by Johann Wolfgang Goethe-Universität Frankfurt a.M. (1991), pp. 51–59
19. R. Busz, P. Gercke (eds.), *Türkis und Azur: Quarzkeramik im Orient und Okzident; [anläßlich der Sonderausstellung vom 18. Juli bis 3. Oktober 1999 im Ballhaus am Schloß Wilhelmshöhe und in Schloß Wilhelmsthal, Souterrain]* (Staatliche Museen Kassel, Ballhaus Kassel, und Schloss, Wolfratshausen: Ed. Minerva, 1999)
20. J.L. Mass, M.T. Wypyski, R.E. Stone, Malkata and Lisht glassmaking technologies: towards a specific link between second millennium BC metallurgists and glassmakers. Archaeometry. **44**(19), 67–82 (2002)
21. C. Berthold, M. Keuper, K. Bente, Dealing with antique objects: Non-destructive X-ray microdiffraction coupled with μ-Raman spectroscopy and μ-X-ray fluorescence. In *Archäometrie und Denkmalpflege*, ed. by T. Gluhak, S. Greiff, K. Kraus, M. Prange, vol. 7 (Mainz, 2015), pp. 24–26
22. G.A. Wagner (ed.), *Einführung in die Archäometrie*. (Springer, Berlin, 2007), p.374
23. S. Klein, G.P. Brey, S. Durali-Müller, Y. Lahaye, Characterisation of the raw metal sources used for the production of copper and copper-based objects with copper isotopes. Archaeol. Anthropol. Sci. **2**(1), 45–56 (2010). https://doi.org/10.1007/s12520-010-0027-y
24. S. Klein, T. Rose, K.J. Westner, Y.-K. Hsu, From OXALID to GlobaLID: a substantial upgrade of a well-known data pool of lead isotopes for metal provenancing using R and Shiny App. In *Abstract book EMC2020* (Krokow, 2021), pp. 210–210
25. K.J. Westner, T. Rose, S. Klein, Y.-K. Hsu, GlobaLID: global lead isotope database. GFZ Data Serv. (2021). https://doi.org/10.5880/FIDGEO.2021.031
26. G. Weiß, Die historische entwicklung der glasurrezepte. Berl. Beitr. Archäometrie. **5**, 97–104 (1980)
27. C.L. Reedy, Petrographic and image analysis of thin sections of classic wares of song dynasty. In *International Symposium on Science and Technology of Five Great Wares of the Song Dynasty*, Beijing (2016)
28. J. Molera, M. Vendrell-Saz, M. García-Vallés, T. Pradell, Technology and colour development of Hispano-Moresque lead-glazed pottery. Archaeometry. **39**(1), 23–39 (1997)
29. A. Hauptmann, R. Busz, S. Klein, A. Vettel, R. Werthmann, The roots of glazing techniques: copper metallurgy? Paleo. **26**(2), 113–129 (2000). https://doi.org/10.3406/paleo.2000.4714
30. R. Di Febo, J. Molera, T. Pradell, O. Vallcorba, J.C. Melgarejo, C. Capelli, Thin-section petrography and SR-μXRD for the identification of micro-crystallites in the brown decorations of ceramic lead glazes. Eur. J. Mineral. **29**(5), 861–870 (2017). https://doi.org/10.1127/ejm/2017/0029-2638
31. J. Molera, T. Pradell, N. Salvadó, M. Vendrell-Saz, Interactions between clay bodies and lead glazes. J. Am. Ceram. Soc. **84**(5), 1120–1128 (2001)
32. J. Molera, V. Martínez Ferreras, A. Fusaro, J.M. Gurt Esparraguera, M. Gaudenzi, S.R. Pidaev, T. Pradell, Islamic glazed

wares from ancient Termez (southern Uzbekistan). Raw materials and techniques. J. Archaeol. Sci. Rep. **29**, 102169 (2020)
33. M.S. Tite, I. Freestone, R. Mason, J. Molera, M. Vendrell-Saz, N. Wood, Lead glazes in antiquity? methods of production and reasons for use. Archaeometry. **40**(2), 241–260 (1998)
34. R. Di Febo, J. Molera, T. Pradell, J.C. Melgarejo, J. Madrenas, O. Vallcorba, The production of a lead glaze with galena: thermal transformations in the PbS–SiO_2 system. J. Am. Ceram. Soc. **101**(5), 2119–2129 (2018)
35. R. Di Febo, J. Molera, T. Pradell, O. Vallcorba, C. Capelli, Technological implications of neo-formed hematite crystals in ceramic lead glazes. STAR Sci. Technol. Archaeol. Res. **3**(2), 366–375 (2017)
36. K.L. Rasmussen, G.R. Milner, Th. Delbey, L.K.I. Jensen, F. Witte, Th. Rehren, U. Kjaer, P. Grinder-Hansen, Release of lead from Renaissance lead-glazed ceramics from southern Denmark and northern Germany: implications from acetic acid etching experiments. Herit. Sci. **10**(1), 63 (2022). https://doi.org/10.1186/s40494-022-00703-8